Analyst

PAPER

View Article Online
View Journal

Cite this: DOI: 10.1039/c4an01463d

Electrochemical immunosensor assay (EIA) for sensitive detection of *E. coli* O157:H7 with signal amplification on a SG–PEDOT–AuNPs electrode interface

Yuna Guo,[a] Yu Wang,*[b] Su Liu,[c] Jinghua Yu,[a] Hongzhi Wang,[a] Min Cui[a] and Jiadong Huang[ab]

A novel electrochemical immunosensor assay (EIA) for highly sensitive and specific detection of *Escherichia coli* O157:H7 has been developed. This immunosensor is constructed by the assembly of capture antibody on SG–PEDOT–AuNPs composites modified glass carbon electrode. In the presence of target *E. coli* O157:H7, horseradish peroxidase (HRP)-labeled antibody is captured on the electrode surface to form a sandwich-type system *via* the specific identification. As a result, *E. coli* O157:H7 detection is realized by outputting a redox current from electro-reduction of hydrogen peroxide reaction catalyzed by HRP. In our assay, the combination of the unique properties of sulfonated graphene (SG) and gold nanoparticles (AuNPs) can not only accelerate electron transfer on electrode interface, but also provide an excellent scaffold for the conjugation of capture antibody that significantly improves the target capture efficiency and enhances the sensitivity of the biosensor. The results reveal the calibration plot obtained for *E. coli* O157:H7 is approximately linear from 7.8 × 10–7.8 × 10^6 colony-forming unit (cfu) mL^{-1} with the limit of detection of 3.4 × 10 cfu mL^{-1}. In addition, the biosensor has been successfully applied to the quantitative assay of *E. coli* O157:H7 in synthetic samples (spring water and milk). Hence, the developed electrochemical-based immunosensor might provide a useful and practical tool for *E. coli* O157:H7 determination and related food safety analysis and clinical diagnosis.

Received 9th August 2014
Accepted 18th October 2014

DOI: 10.1039/c4an01463d

www.rsc.org/analyst

1. Introduction

Microbiological contamination caused by food-borne diseases has become a major public health problem in the world.[1,2] The Centers for Disease Control and Prevention estimates that there are 76 million cases of food-borne illness each year in the United States.[3] Among the pathogenic bacteria, *Escherichia coli* O157:H7 (*E. coli* O157:H7) is one of the most detrimental food pathogens that can cause serious food-borne illness and even death.[3,4] Therefore, there is an urgent need to develop simple, rapid and cost-efficient strategies for the sensitive and specific determination of *E. coli* O157:H7.

Conventionally, pathogenic bacteria identification is performed using a culturing-based method, which involves selective culture, Gram staining, as well as biochemical and serological tests.[5] Colony count estimation provides an inexpensive technique for pathogenic bacteria determination with simple operation. However, this procedure is rather time-consuming to obtain visible colonies that can be identified. Recent efforts in developing novel non-culture based strategies includes enzyme linked immunosorbent assay (ELISA),[6,7] polymerase chain reaction (PCR),[8,9] protein microassays,[10] quartz crystal microbalance (QCM) system,[11] surface plasmon resonance (SPR),[12,13] and flow cytometry[14]-based assay methods. For example, PCR-based assays involve the amplification and subsequent analysis of pathogen-specific nucleic acid by PCR and sequencing, which have the ability of simultaneous analysis of multiple pathogens. However, a major disadvantage of this assay is its susceptibility to external factors such as complex sample matrices, non-specific DNA amplification and so on. Protein microassays as alternative tools for pathogen detection offer convenient techniques for high-throughput screening of bacterial isolates from numerous sample matrices. Nevertheless, it can't be ignored that this approach demands high testing cost. Therefore, these new techniques-based assay methods may combine some appealing features such as multiplexing ability, excellent sensitivity or rapid detection. However, they may suffer from some intrinsic limitations such as requirement of skilled technical staff and expensive equipment or reagents.

[a]*Key Laboratory of Chemical Sensing & Analysis in Universities of Shandong, School of Chemistry and Chemical Engineering, University of Jinan, Jinan 250022, P.R. China*
[b]*School of Biological Sciences and Technology, University of Jinan, Jinan 250022, P.R. China. E-mail: bio_wangy@ujn.edu.cn; Fax: +86-531-82769122; Tel: +86-531-89736122*
[c]*School of Resources and Environment, University of Jinan, Jinan 250022, P.R. China*

Immunoassay, the quantitative analysis of antigens or antibodies concentrations based on the highly specific recognition interactions of antibodies and antigens, has been recognized as a very powerful tool in bioanalysis and clinical diagnosis due to its high sensitivity, superb specificity and possible analysis of difficult matrices without extensive pretreatment.[15,16] Among the various immunosensors developed, the electrochemical immunosensor assay (EIA) has gained considerable attention as a bioanalytical technique owing to its high detection speed, excellent compatibility, minimal sample consumption, low cost and power requirements, and ease of miniaturization.[17,18] In view of these merits, EIA methods seem to be suitable for practical applications. Typically, the electrochemical-based immunoassay is performed using a sandwich-type immunoassay, which involves the recognition elements (antibodies or antigens) immobilized on the electrode surface to combine with target analytes and result in signal amplification and reading due to immunological responses.[19] In recent years, great efforts have been focused on the development of effective signal amplification strategies to meet the increasing demand for ultrasensitive detection of analytes.[20,21] With the remarkable development of nanotechnology, new nanomaterials have been extensively used to improve the sensitivity of biosensor such as graphene (GR), carbon nanotubes, conducing polymers, metal nanoparticles and so on.[22–25]

GR, a single layer sp^2 carbon network arranged in a perfect honeycomb lattice, has opened a new path for the utilization of 2D carbon materials as supports.[22] Because of its unique properties, such as high surface-to-volume ratio, excellent electronic conductivity, easy functionalization and remarkable chemical stability, GR has been recognized as an ideal electroactive species in constructing composite materials for biosensing applications.[26,27] Typically, GR is acquired by chemical reduction or thermal reduction from graphene oxide (GO) with harsh reducing agents such as hydrazine monohydrate.[28] However, the reduced graphene oxide (rGO) often suffers from irreversible cohesion due to van der Waals interactions, which adversely affects the electrochemical performance as a result of hindering electrolyte penetration into layers.[29] It has been reported that surface functionalization of GR with polymers can be used as an effective approach to resolve such problems.[30] For example, poly-(3,4-ethylenedioxythiophene) (PEDOT), a conducting polymer, has been widely applied in GR surface functionalization owing to its excellent film-forming property.[31]

The multivalent recognition effect is recognized as a very effective approach to achieve improved affinity.[32] Recently, a wide variety of nanoparticles, such as dendrimers,[33] gold nanoparticles (AuNPs),[34] quantum dots[35] for antibodies, peptides, and DNA, have been developed to be used as scaffolds. Among them, AuNPs have attracted considerable attention because of their unique properties, such as easy synthesis, huge interfaces for biomolecules, excellent conductivity, good biocompatibility, and desirable chemical stability.[36] The large surface area of nanoparticles improves the loading capability of active biomolecules that enhances the recognition ratio and binding affinity.

Herein, we report the development of a novel EIA for sensitive and specific detection of *E. coli* O157:H7. Sulfonated graphene (SG)–PEDOT–AuNPs composites are successfully synthesized *via* a simple one-step reaction. This biosensor is constructed by the assembly of capture antibody on the surface of SG–PEDOT–AuNPs composite modified glass carbon electrode (GCE). After the sandwich-type identification, *E. coli* O157:H7 detection is realized by outputting a redox current from electro-reduction of hydrogen peroxide reaction catalyzed by horseradish peroxidase (HRP). In our work, the combination of the unique properties of SG and AuNPs can not only accelerate electron transfer rate on the electrode interface, but provide an excellent scaffold for the conjugation of capture antibody that remarkably improves the target capture efficiency and enhances the sensitivity of the biosensor as well. Moreover, the use of antibody offers high specificity intrinsic to the immuno-recognition, which also improves binding efficiency and enhances the selectivity of the biosensor. Furthermore, the proposed biosensor overcomes the limitations of previously reported methods,[6–14] and provides simple, rapid, and cost-effective detection of *E. coli* O157:H7 with high sensitivity and selectivity. Hence, the developed electrochemical-based immunosensor might provide a useful and practical tool for *E. coli* O157:H7 determination and related food safety analysis and clinical diagnosis.

2. Experimental section

2.1 Reagents and materials

Rabbit anti-*E. coli* O157:H7 antibody (capture antibody) and horseradish peroxidase-labeled mouse anti-*E. coli* O157:H7 antibody (HRP-labeled antibody) were purchased from Shanghai Prajna Biology Technique Ltd. (Shanghai, China). *E. coli* O157:H7, Salmonella, *E. coli* DH5α and *E. coli* O149 were obtained from Institute of Microbiology Chinese Academy (Beijing, China). Peptone, beef extract powder, bacto-tryptone and bacto-yeast extract were obtained from Qingdao Biological Technology Co. Ltd. (Qingdao, China). 3,4-Ethylenedioxythiophene (EDOT), styrenesulfonate (PSS), graphite and bovine serum albumin (BSA) were purchased from Sigma Aldrich Corporation (St. Louis, MO, USA). Gold chloride trihydrate ($HAuCl_4 \cdot 3H_2O$), disodium hydrogen orthophosphate ($Na_2HPO_4 \cdot 12H_2O$) and sodium dihydrogen orthophosphate ($NaH_2PO_4 \cdot 2H_2O$) were obtained from Aladdin Chemistry Co. Ltd. (Shanghai, China). All other chemicals were of analytical grade and obtained from Sinopharm Chemical Reagent Co. Ltd. (Beijing, China). All solutions were prepared using ultrapure water, which was obtained through a Millipore Milli-Q water purification system (Billerica, MA, USA) and had an electric resistance > 18.3 MΩ. Milk and spring water samples were obtained from a local market.

2.2 Apparatus

Cyclic voltammetry (CV) and differential pulse voltammetry (DPV) were carried out on a CHI 660D electrochemical workstation (Shanghai Chen Hua Instrument Co. Ltd., China) with a

conventional three-electrode system composed of a bare or functionalized GCE (~3 mm diameter) as the working electrode, a platinum wire as the auxiliary electrode (~0.1 mm diameter), and a Ag/AgCl reference electrode with saturated KCl solution as the reference electrodes. UV-vis spectra were recorded using a Lambda 35 Spectrometer (Perkin Elmer, USA) in the wavelength range from 200–750 nm. Fourier transform infrared (FTIR) spectra were recorded using Spectrum One FTIR apparatus (Perkin Elmer, USA). Scanning electron microscope (SEM) images were obtained from field emission SEM (ZEISS, Germany). The pH value of the used buffer was measured by a FE 20 Mettler-Toledo pH meter (Switzerland).

2.3 Synthesis of SG

GO was synthesized from natural graphite according to the Hummers method[37] with slight modifications as follows: 100 mg GO was dispersed in water and treated with ultrasonication at RT for 2 h. The pH value of the solution was adjusted to 9–10 with 5% (wt%) sodium hydroxide solution. After the addition of a 6 mL of 10 mM $NaBH_4$ solution, the mixture was refluxed at 80 °C for 12 h under constant stirring. The colour of resulting solution changed from deep brown to black. Then the black RGO was collected by centrifugation and repetitively rinsed with ultrapure water and ethanol and dried at 60 °C in a vacuum for 24 h.

Subsequently, 50 mg RGO was added to a 8 mL of 10 mM sulfanilic acid solution followed by mild mixing at room temperature (RT) for 6 h. The resulting solution was mixed with 5 mL sodium nitrite solution (100 mM, containing 1 M HCl) and gently stirred at 4 °C for 2 h. Then the produced precipitates were purified by washing several times with ultrapure water and methanol until the filtrate was colorless and attained a neutral pH. The as-prepared SG was collected by vacuum filtration.

2.4 Preparation of SG–PEDOT–AuNPs composites

The SG–PEDOT–AuNPs aqueous dispersion was synthesized by the reduction of $HAuCl_4$ with EDOT monomer in the presence of SG and PSS. 25 mL aqueous solution of EDOT (15 mM) and 3 mL of 1% (w/v) PSS were added into 25 mg as-prepared SG and adequately stirred at RT for 0.5 h. Then 10 mL $HAuCl_4$ solution (6.25 mM) was added drop wise into the mixture solution with vigorous stirring. After reaction at RT for 12 h, the dispersion solution was centrifuged at 8000 rpm for 5 min to remove the surplus reagents. Subsequently, the produced solids were washed thoroughly with ultrapure water and dried under vacuum conditions to get purified SG–PEDOT–AuNPs composites.

2.5 The fabrication of the biosensor

GCE was polished sufficiently with 0.3 and 0.05 μm alumina powder on a microcloth, followed by rinsing with ultrapure water and ethanol. The SG–PEDOT–AuNPs composites were dispersed into ultrapure water with ultrasonication to get homogeneous solution at concentration of 1.0 mg mL^{-1}. Then, the pretreated GCE was decorated with SG–PEDOT–AuNPs composites by the addition of 10 μL of the as-prepared solution, followed by drying at RT for 2 h. Subsequently, 10 μL of 0.5 mg mL^{-1} capture antibody solution was added and incubated on the surfaces of SG–PEDOT–AuNPs/GCE at RT for 2 h, followed by wash with 10 mM phosphate buffer solution (PBS) (pH 7.4). To block extra sites and reduce non-specific adsorption, 10 μL of 5% BSA solution was deposited on the modified electrode surface and incubated at RT for 2 h. Finally, the fabricated electrode was rinsed with PBS and made ready for use.

2.6 Immunoassay procedure for detection of *E. coli* O157:H7

E. coli O157:H7 were cultured aerobically in lysogeny broth media (LB: bacto-tryptone 12 g; bacto-yeast extract 6 g; and NaCl 7 g) at 37 °C for 24 h. The suspensions were stored at 4 °C and brought to RT just before use. The number of *E. coli* O157:H7 was counted over a time course of 24 h by the plate counting method. The immunoassay was performed using a typical sandwiched immunoassay procedure. 10 μL of different concentrations of *E. coli* O157:H7 solution were added and incubated with the fabricated electrodes at 37 °C for 60 min followed by washing with PBS. Then, 10 μL of 0.5 mg mL^{-1} HRP-labeled antibody solution was deposited and incubated with the electrodes at 37 °C for 60 min. After washing three times with PBS, the electrodes were immersed into the working solution to perform electrochemical measurements. All electrochemical measurements, including DPV and CV, were performed at RT using a three-electrode system consisting of a Ag/AgCl reference electrode, a platinum counter electrode and the working electrode. DPV measurement was carried out in 10 mM PBS (pH 7.4) containing 3 mM HQ and 1.5 mM H_2O_2 within the potential range from −0.15 V to 0.2 V with a pulse height of 50 mV and the step height and the frequency were kept as 4 mV and 15 Hz, respectively. CV was performed in 10 mM PBS solution containing 5.0 mM $K_3[Fe(CN)_6]$ within the potential range from −0.2 to 0.6 V using a step potential 10 mV at a scan rate of 50 mV s^{-1}.

3. Results and discussion

3.1 Design strategy of the electrochemical immunosensor

Scheme 1 illustrates the concept for the proposed electrochemical-based immunoassay strategy. The preparation process of SG–PEDOT–AuNPs composites is shown in scheme 1A. SG dispersion can be carried out by the modification of sulfonic acid groups on the surface of GR through covalent interactions. SG–PEDOT–AuNPs composites can be readily synthesized by a one-step reaction at RT using $HAuCl_4$ as an oxidant. PEDOT and PSS, two conducting polymers, which possess the merits of excellent film-forming property, high electrical conductivity, desirable stability, and good biocompatibility, are used for surface functionalization of SG.[38] Because the PEDOT backbone contains aromatic thiophene rings, it can be coupled to the surface of SG *via* strong π–π stacking interactions.[39] Particularly, PSS is used to promote PEDOT to disperse into an aqueous medium, which also acts as the source for the charge-balancing counterions.[40] The design principles of the proposed biosensor are shown in scheme 1B. The as-prepared SG–PEDOT–AuNPs composites are coated onto

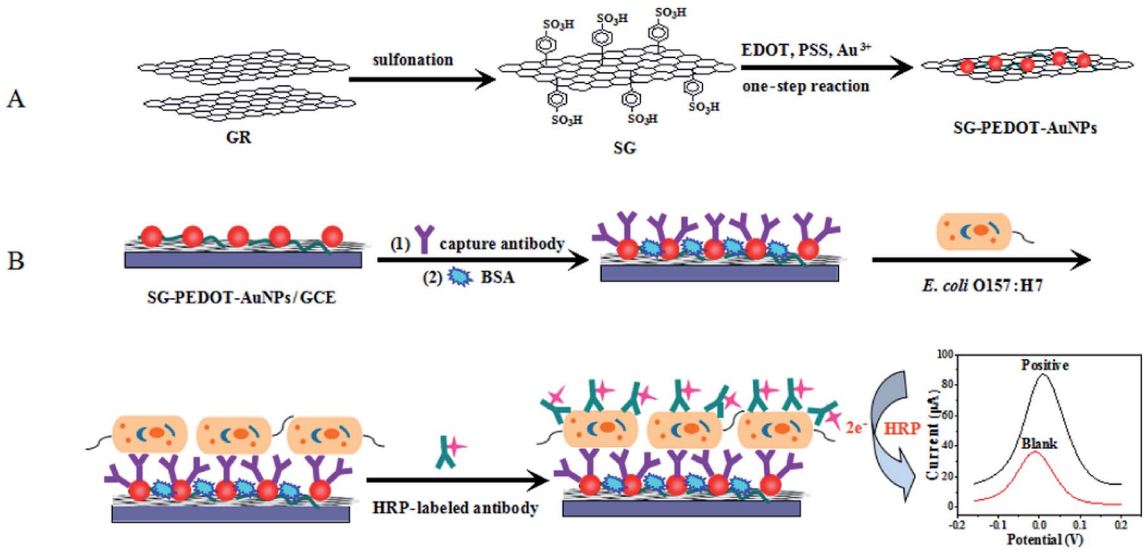

Scheme 1 (A) Schematic representation of the preparation of SG–PEDOT–AuNPs composites. (B) Schematic representation of EIA for sensitive detection of *E. coli* O157:H7 with signal amplification on a SG–PEDOT–AuNPs electrode interface.

the surface of the GCE, which can not only enhance interface electron transfer efficiency, but also offers an excellent mediator for a facilitated multivalency effect that allows to conjugate more active biomolecules. The immunosensor is fabricated by immobilizing a capture antibody on SG–PEDOT–AuNPs composites modified by GCE *via* electrostatic interaction. Furthermore, BSA is further assembled on the surface of electrode to block extra active sites and reduce non-specific adsorption. When the as-prepared electrode is incubated in the presence of *E. coli* O157:H7, a sandwich-type system can be constructed *via* the specific identification, which results in the HRP-labeled antibody being placed close to the electrode surface. After the addition of substrate solution, a strong redox current signal from the electro-reduction of H_2O_2 reaction catalyzed by HRP is obtained, which corresponds to the concentration of *E. coli* O157:H7.

3.2 Electrochemical behaviors

To test the feasibility of the proposed method, DPV measurements were performed in 10 mM PBS containing 1.5 mM H_2O_2 and 3 mM HQ. Fig. 1A depicts typical DPV responses of the biosensor in the assay of *E. coli* O157:H7. When the electrode was incubated in the presence of *E. coli* O157:H7, it was observed that a strong peak current appeared in the DPV curves, indicating that the HRP-labeled antibody combined to the electrode surface and catalyzed the electro-reduction of H_2O_2 reaction (curve a). In contrast, a very weak DPV peak current was obtained after incubation in the absence of *E. coli* O157:H7, which was attributed to the absence of HRP-labeled antibody on the surface of electrode (curve b). This clearly revealed that the enhanced DPV signal was induced by specific immunological recognition events rather than non-specific interactions.

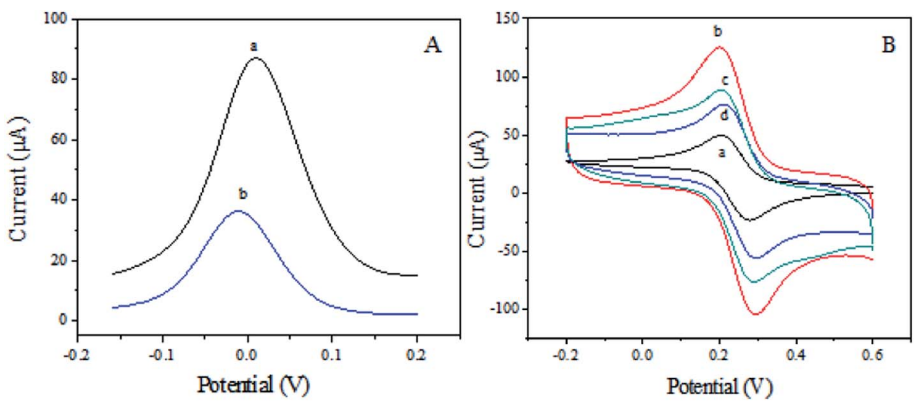

Fig. 1 (A) DPVs of the biosensor obtained in 10 mM PBS (pH 7.4) containing 3 mM HQ and 1.5 mM H_2O_2 before (b) and after (a) reaction with 7.8 $\times$ 10^4 cfu mL^{-1} *E. coli* O157:H7. (B) CVs obtained for the bare GCE (a), SG–PEDOT–AuNPs/GCE (b), capture antibody/SG–PEDOT–AuNPs/GCE (c), BSA/capture antibody/SG–PEDOT–AuNPs/GCE (d). Measurements were performed in 10 mM PBS (pH 7.4) containing 0.25 mM KCl and 5.0 mM $K_3[Fe(CN)_6]$.

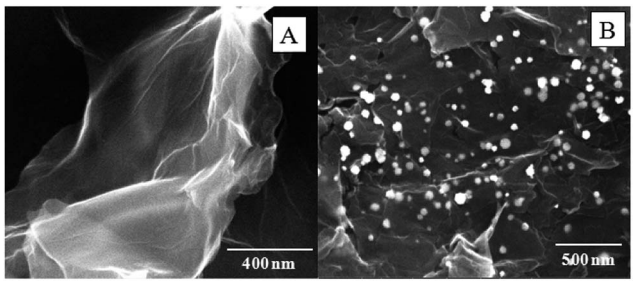

Fig. 2 (A) SEM image of SG deposited on GCE. (B) SEM image of SG–PEDOT–AuNPs composites deposited on GCE.

The modification of the sensing interface of the electrode was of great importance to improve the analytical performance of the biosensor. We performed CV measurements to monitor the fabrication process of electrode, as shown in Fig. 1B. With the bare GCE, a pair of well-defined redox peaks appeared at 0.17 mV and 0.26 mV, a typical redox peak range of $K_3[Fe(CN)_6]$ (curve a). With the electrode modified by SG–PEDOT–AuNPs composites, there was a significantly increased peak current in the CV curves (curve b). This signified that the SG–PEDOT–AuNPs composites effectively facilitated the electron transfer between electrode and solution due to its excellent electronic conductivity. After modifying with capture antibody, an evidently decreased CV signal was observed, indicating the electron transfer was hindered by the isolated bio-macromolecules (curve c). To block extra active sites, BSA was immobilized on the surface of electrode. It was observed that a weaker current peak appeared in the CV curves, which demonstrated that BSA was bound to the electrode surface and further hindered the access of the redox probe to the electrode surface (curve d). On the basis of these results, it was reasonably concluded that the fabrication of the sensing interface for *E. coli* O157:H7 was successfully achieved.

3.3 Characterization of SG–PEDOT–AuNPs composites

SEM was employed to investigate the morphology and micro-structure of the as-prepared nanocomposites, as shown in Fig. 2. We observed from the image that SG displayed the typically flake-like structure with slightly crumpled and wrinkled edge (Fig. 2A). With the electrode modified by SG–PEDOT–AuNPs composites, it was found that a large number of bright dots, AuNPs with an average diameter of ~13 nm, appeared on the entire surface of SG, particularly at the folded edges and wrinkled sites (Fig. 2B). This showed that the SG–PEDOT–AuNPs composites was successfully synthesized and deposited evenly on the surfaces of GCE. The formation of homogeneous composites solution benefited from the excellent film-forming ability of PEDOT and PSS, which could effectively prevent the reduced SG from restacking. Because of the combination of the unique properties of SG and AuNPs, the SG–PEDOT–AuNPs composites could not only enhance electron transfer rate on electrode interface, but offer a large specific surface area for the conjugation of capture antibody and improve the sensing performance of the biosensor as well.

UV-vis spectroscopy analysis was performed to confirm the formation of SG–PEDOT–AuNPs composites and the results are shown in Fig. 3A. We observed that a sharp adsorption peak appeared at 260 nm, which was assigned to the $\pi \rightarrow \pi^*$ transition of pyridine heterocycle (curve a). For SG–PEDOT–AuNPs composites solution, there was a new adsorption peak centered at 522 nm, typical for individual AuNPs of ~13 nm (curve b), which was consistent with the result of SEM characterization. These results demonstrated the accomplishment of the SG–PEDOT–AuNPs composites.

We further utilized FTIR spectra to inspect the molecular structure of the as-prepared composites, as shown in Fig. 3B. From the FTIR spectrum of pure SG (curve a), the adsorption at 1113 and 1050 cm^{-1} could be assigned to the S–O stretching vibrations, whereas the adsorption peaks at 1155 and 3420 cm^{-1} could be corresponded to S-phenyl and –OH stretching vibrations, respectively. These data confirmed that the surface of GR was successfully decorated with sulphonic groups.[41] The spectrum also showed other adsorption peak at 1630 cm^{-1}, which could be assigned to the skeletal vibration of SG. From the FTIR spectrum of SG–PEDOT–AuNPs composites (curve b), it was found that two adsorption peak appeared at 1485 and 1272 cm^{-1}, which were attributed to the C=C and C–C

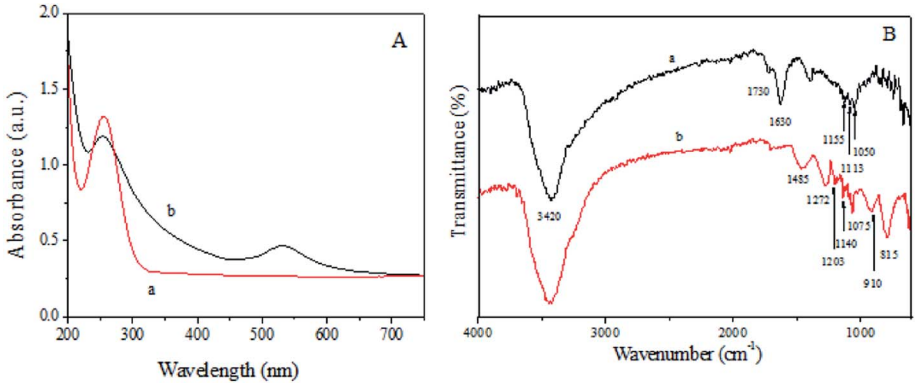

Fig. 3 (A) UV-vis spectroscopy obtained for SG (a) and SG–PEDOT–AuNPs composites (b). (B) FTIR spectra obtained for SG (a) and SG–PEDOT–AuNPs composites (b).

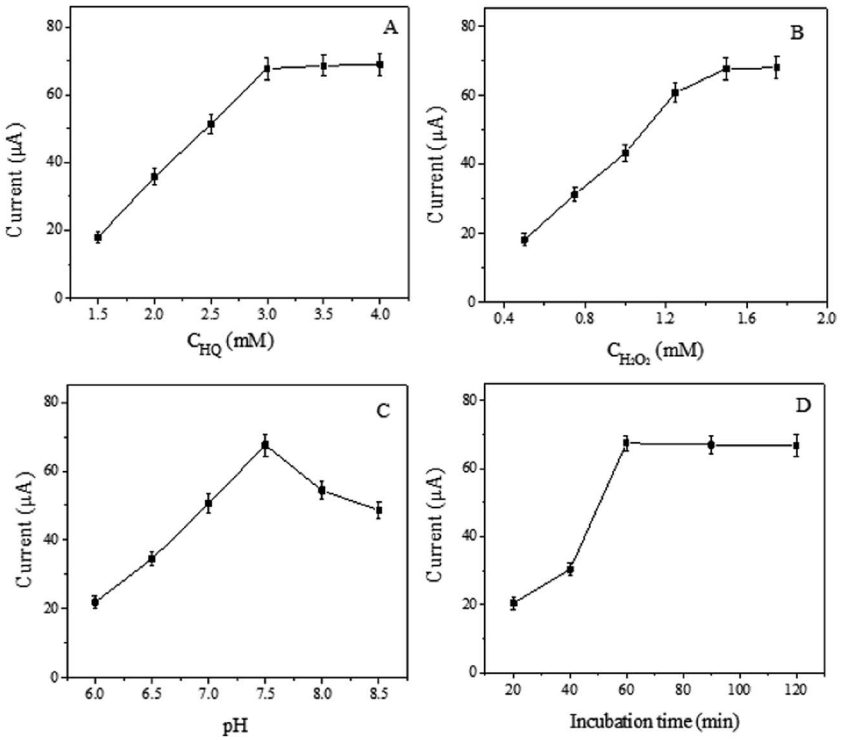

Fig. 4 (A) Effect of the concentrations of HQ on the DPV peak current of biosensor. (B) Effect of the concentrations of H_2O_2 on the DPV peak current of biosensor. (C) Effect of the pH values of the working solution on the DPV peak current of biosensor. (D) Effect of the incubation time of *E. coli* O157:H7 on the DPV peak current of biosensor. The concentration of *E. coli* O157:H7 is 7.8×10^4 cfu mL^{-1}. Error bars are standard deviations across three repetitive experiments.

stretching of thiophene ring, respectively. There were other adsorption peaks at 815 and 920 cm^{-1}, which corresponded to vibration modes of C–S bond of thiophene ring. The adsorption peak at 1630 cm^{-1} nearly became invisible because of reduced concentration of SG for the synthesized composites compared to pure SG.[42] A new adsorption peak at 1140 cm^{-1} was ascribed to the stretching mode of the ethylenedioxy group. The spectrum also displayed two adsorption peaks located at 1075 and 1203 cm^{-1}, which were assigned to the stretching vibration of the sulfone groups SO_2 and SO_3^-, respectively. These data verified the formation of SG–PEDOT–AuNPs composites.

3.4 Optimization of experimental conditions

The maximized current responses of the biosensor are significantly influenced by the concentrations of HQ and H_2O_2, which are the substrates of the HRP-catalyzed redox reaction. The current responses to the different concentrations of HQ were investigated, as shown in Fig. 4A. It was observed that the current signal increased with the increase of HQ concentration and reached equilibrium when the concentration was 3 mM. Therefore, a HQ concentration of 3 mM was used for the following experiments. Similar results were obtained for the concentration of H_2O_2 (Fig. 4B), and a H_2O_2 concentration of 1.5 mM was chosen as the optimal concentration.

It is also important for the pH value of the working solution to achieve maximum current signal. The results in Fig. 4C show that the current signal depends on the pH of the electrolyte. It was observed that the current increased when the pH increased from 6.0 to 7.4 and then decreased when the pH was further increased to 8.5. As a result, the pH of 7.4 was selected for the detection.

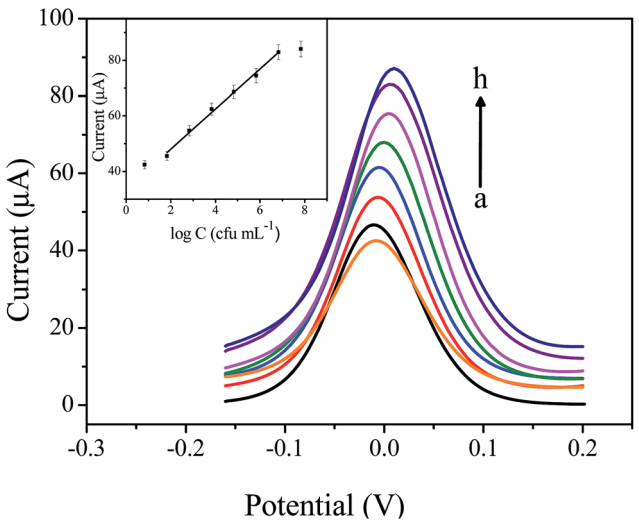

Fig. 5 (A) Typical DPV responses of the biosensor to different concentrations of *E. coli* O157:H7 (from curve a to h: 0, 7.8×10, 7.8×10^2, 7.8×10^3, 7.8×10^4, 7.8×10^5, 7.8×10^6, 7.8×10^7 cfu mL^{-1}). The inset is the calibration curve of DPV peak currents for different *E. coli* O157:H7 concentrations. Error bars are standard deviations across three repetitive experiments.

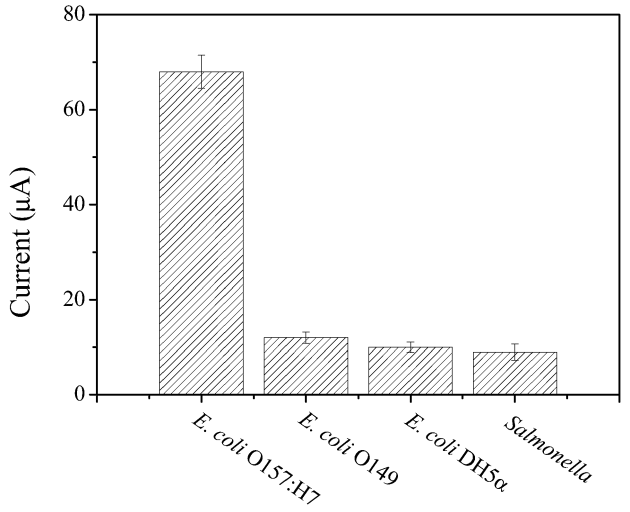

Fig. 6 DPV peak currents for different bacteria (10^6 cfu mL^{-1}). The concentration of *E. coli* O157:H7 is 7.8×10^4 cfu mL^{-1}. Error bars are standard deviations across three repetitive experiments.

The effect of the incubation time of the *E. coli* O157:H7 on the modified electrode was also investigated. As shown in Fig. 4D, the current signals increased with the increase of incubation time and reached equilibrium when the incubation time was 60 min. Therefore, the optimal incubation time for the electrode was chosen to be 60 min for the target capture.

3.5 Analytical performance of the immunosensor for *E. coli* O157:H7 detection

3.5.1 Calibration curve. Under the optimized conditions, the fabricated biosensor was adopted for the determination of a series of different concentrations of *E. coli* O157:H7. Fig. 5 shows the typical DPV responses of the biosensor to *E. coli* O157:H7 of varying concentration. We observed that the peak current increased in response to increasing concentrations of *E. coli* O157:H7 and was proportional to the logarithmic value of the *E. coli* O157:H7 concentration within the range from 7.8×10–7.8×10^6 cfu mL^{-1}. A linear regression equation ($I = 33.68 \log[C_{E.\ coli}$ (cfu mL^{-1})] + 7.19) was obtained in the concentration range from 7.8×10–7.8×10^6 cfu mL^{-1} with a detection limit of 3.4×10 cfu mL^{-1} at 3σ. In addition, the analytical performance of the proposed immunosensor in the quantitative assay of *E. coli* was compared with that of some previously reported methods.[5,7,9,11,13] The results are shown in Table 1. It was observed that our EIA-based strategy displayed higher sensitivity and wider linear range compared to these methods. Therefore, we might conclude that the proposed biosensor is potentially useful for the quantitative assay of *E. coli* O157:H7 with desirable sensitivity and reproducibility.

3.5.2 The selectivity, reproducibility and stability of the immunosensor. The selectivity of the biosensor for *E. coli* O157:H7 assay was also investigated using non-target bacteria such as Salmonella, *E. coli* DH5α and *E. coli* O149. As shown in Fig. 6, the results revealed these non-target bacteria had slight interference with this biosensor. This indicated the proposed biosensor exhibited superb specificity towards *E. coli* O157:H7.

To investigate the reproducibility of the biosensor, five electrodes made using the same fabrication procedure were utilized to determine 7.8×10^4 cfu mL^{-1} *E. coli* O157:H7. The current responses showed a relative standard deviation (RSD) of 3.4% for five independent measurements. This indicated that the preparation process yielded a biosensor showing very good reproducibility.

Stability is one of the important parameters for practical application of biosensor, and it was also evaluated in this work.

Table 1 Comparison of different assay methods for *E. coli* O157:H7 determination

Detection methods	Detection time	Detection range (cfu mL^{-1})	Detection limit (cfu mL^{-1})	Reference
Colony count estimation	24 hours	1.0×10^3–1.0×10^8	1.0×10^3	5
ELISA	6–7 hours	1.0×10^4–1.0×10^7	1.0×10^4	7
PCR	~3 hours	1.2×10^3–1.2×10^8	1.2×10^3	9
QCM	2–3 hours	1.0×10^2–1.0×10^5	1.0×10^2	11
SPR	~2 hours	1.25×10^2–1.25×10^7	1.25×10^2	13
EIA	~2.5 hours	7.8×10–7.8×10^6	3.4×10	This work

Table 2 *E. coli* O157:H7 analysis in synthetic samples

Samples	Spiked amount (cfu mL^{-1})	Sensor (cfu mL^{-1})	Recovery (%)	Plate count method (cfu mL^{-1})
Spring water	7.8×10^2	$(7.57 \pm 0.36) \times 10^2$	97.1	7.98×10^2
	7.8×10^3	$(8.03 \pm 0.29) \times 10^3$	103.0	7.41×10^3
	7.8×10^4	$(7.12 \pm 0.23) \times 10^4$	91.3	7.53×10^4
Milk	7.8×10^2	$(7.37 \pm 0.31) \times 10^2$	94.5	8.09×10^2
	7.8×10^3	$(7.62 \pm 0.33) \times 10^3$	97.7	7.97×10^3
	7.8×10^4	$(7.17 \pm 0.28) \times 10^4$	91.9	8.21×10^4

Five electrodes were fabricated independently under the same conditions and stored at 4 °C for 2 weeks. Then these electrodes were used to detect 7.8×10^4 cfu mL^{-1} *E. coli* O157:H7. The results showed that about 92% of its initial response of the biosensor for *E. coli* O157:H7 remained, indicating this biosensor had very desirable stability.

3.6 Real sample analysis

The feasibility of the proposed biosensor for quantitative assay of *E. Coli* O157:H7 in synthetic samples (spring water and milk) was also investigated. Different concentrations of *E. coli* O157:H7 were spiked into two samples (10× diluted with PBS buffer). Table 2 shows the results in the assays for the synthetic samples. It was found that the recovery of the biosensor was in the range of 91.3–103.0%. In addition, the synthetic samples were further quantified by a classic plate count method. These data obtained using our biosensor strategy were in good agreement with those obtained *via* the plate count method, and the discrepancies between the plate count method and our method were all smaller than 13%. This clearly demonstrated the potential of our biosensor for applications in complicated samples.

4. Conclusions

In this work, we developed a novel EIA for sensitive and specific determination of *E. coli* O157:H7 based on SG–PEDOT–AuNPs composites. The composites could not only accelerate the electron transfer rate on the electrode interface, but offer a multivalent recognition interface for the conjugation of *E. coli* O157:H7 as well. Moreover, the use of antibody offers high specificity intrinsic in the immuno-recognition, which also improves binding efficiency and enhances the selectivity of the biosensor. In addition, this biosensor was also used to analyse *E. coli* O157:H7 in synthetic samples, and the results were well consistent with the plate count method. Compared with existing techniques for *E. coli* detection, such as ELISA and other previous reported methods,[6–14] our EIA-based biosensing strategy offered improved sensitivity and widened linear range. Moreover, the proposed approach had the advantages of simplicity, time efficiency, easy preparation, and low cost detection with high stability. Thus, the proposed electrochemical-based immunoassay might create a new platform for the quantification of *E. coli* O157:H7 and related food safety analysis and clinical diagnosis.

Acknowledgements

This work was supported by the National High Technology Research and Development Program of China (2012AA101604) and the National Natural Science Foundation of China (31171700 and 31101296)

References

1 Q. Lu, H. Lin, S. Ge, S. Luo, Q. Cai and C. A. Grimes, *Anal. Chem.*, 2009, **81**, 5846–5850.
2 S. E. Ichi, F. Leon, L. Vossier, H. Marchandin, A. Errachid, J. Coste, N. Jaffrezic-Renault and C. Fournier-Wirth, *Biosens. Bioelectron.*, 2014, **54**, 378–384.
3 Y. Wang, J. Ping, Z. Ye, J. Wu and Y. Ying, *Biosens. Bioelectron.*, 2013, **49**, 492–498.
4 K. Rijal and R. Mutharasan, *Analyst*, 2013, **138**, 2943–2950.
5 E. G. Vellioua, E. Noriega, E. V. Derlindena, L. Mertens, K. Boons, A. H. Geeraerda, F. Devlieghere and J. F. Van Impe, *Food Res. Int.*, 2013, **54**, 1746–1752.
6 H. Sharma and R. Mutharasan, *Anal. Chem.*, 2013, **85**, 3222–3228.
7 N. Wang, M. He and H. C. Shi, *Anal. Chim. Acta*, 2007, **590**, 224–231.
8 M. M. Hoehl, E. S. Bocholt, A. Kloke, N. Paust, F. von Stetten, R. Zengerle, J. Steigert and A. H. Slocum, *Analyst*, 2014, **139**, 2788–2798.
9 B. E. Luedtke, J. L. Bono and J. M. Bosilevac, *J. Microbiol. Methods*, 2014, **105**, 72–79.
10 Y. Liu, W. Zhong, R. J. Li and S. Li, *Molecules*, 2012, **5**, 4770–4781.
11 D. Li, Y. Feng, L. Zhou, Z. Ye, J. Wang, Y. Ying, C. Ruan, R. Wang and Y. Li, *Anal. Chim. Acta*, 2011, **687**, 89–96.
12 J. Homola, *Chem. Rev.*, 2008, **108**, 462–493.
13 I. Yazgan, N. M. Noah, O. Toure, S. Zhang and O. A. Sadik, *Biosens. Bioelectron.*, 2014, **61**, 266–273.
14 T. S. Gunasekera, P. V. Attfield and D. A. Veal, *Appl. Environ. Microbiol.*, 2000, **66**, 1228–1232.
15 R. Tozzoli, M. Bagnasco, D. Giavarina and N. Bizzaro, *Autoimmun. Rev.*, 2102, 107–113.
16 P. Li, Q. Zhang and W. Zhang, *TrAC, Trends Anal. Chem.*, 2009, **28**, 1115–1126.
17 Y. Haesik, *Curr. Opin. Chem. Biol.*, 2012, **16**, 422–428.
18 W. Siangproh, W. Dungchai, P. Rattanarat and O. Chailapakul, *Anal. Chim. Acta*, 2011, **690**, 10–25.
19 G. Lai, F. Yan, J. Wu, C. Leng and H. Ju, *Anal. Chem.*, 2011, **83**, 2726–2732.
20 L. Wang, C. Z. Zhu, L. Han, L. H. Jin, M. Zhou and S. J. Dong, *Chem. Commun.*, 2011, **47**, 7794–7796.
21 S. Singh, A. Kaushal, S. Khare, P. Kumar and A. Kumar, *Analyst*, 2014, **139**, 3600–3606.
22 A. K. Geim, *Science*, 2009, **324**, 1530–1534.
23 I. Capek, *Adv. Colloid Interface Sci.*, 2009, **150**, 63–89.
24 C. Aleman, B. Teixeira-Dias, D. Zanuy, F. Estrany, E. Armelin and L. J. del Valle, *Polymer*, 2009, **50**, 965–1974.
25 X. Gu, W. Gu, B. Y. Chen, K. Zhao and Y. Z. Xian, *Microchim. Acta*, 2014, **181**, 1–22.
26 D. K. James and J. M. Tour, *Acc. Chem. Res.*, 2013, **46**, 2307–2318.
27 Y. T. Wu, L. L. Tang, L. H. Huang, Z. Z. Han, J. Wang and H. B. Pan, *Mater. Sci. Eng., C*, 2014, **39**, 92–99.
28 R. K. Layek, S. Samanta and A. K. Nandi, *Carbon*, 2012, **50**, 815–827.
29 C. Zhang, Z. Zhang and G. Li, *J. Chromatogr. A*, 2014, **1346**, 8–15.
30 L. Yang, H. Yang, L. Wang, B. K. Teh, J. Q. Zhong, H. Chou, L. Chen, W. Chen, Z. Shen and R. S. Ruoff, *ACS Nano*, 2012, **6**, 5941–5951.
31 X. Zhang, C. Li and Y. Luo, *Langmuir*, 2011, **27**, 1915–1923.

32 X. Chen, Y. Wang, Y. Zhang, Z. Chen, Y. Liu, Z. Li and J. Li, *Anal. Chem.*, 2014, **86**, 4278–4286.
33 L. Gu, P. G. Luo, H. Wang, M. J. Meziani, Y. Lin, L. M. Veca, L. Cao, F. Lu, X. Wang, R. A. Quinn, W. Wang, P. Zhang, S. Lacher and Y. P. Sun, *Biomacromolecules*, 2008, **9**, 2408–2418.
34 R. Li, K. Wu, C. Liu, Y. Huang, Y. Wang, H. Fang, H. Zhang and C. Li, *Anal. Chem.*, 2014, **86**, 5300–5307.
35 H. Liu, S. Xu, Z. He, A. Deng and J. Zhu, *Anal. Chem.*, 2013, **85**, 3385–3392.
36 X. Cao, Y. Ye and S. Liu, *Anal. Biochem.*, 2011, **417**, 1–16.
37 W. S. Hummers and R. E. Offeman, *J. Am. Chem. Soc.*, 1958, **80**, 1339.
38 S. J. Li, G. Y. Zhao, R. X. Zhang, Y. L. Hou, L. Liu and H. Pang, *Microchim. Acta*, 2013, **108**, 821.
39 J. Zhou and G. Lubineau, *ACS Appl. Mater. Interfaces*, 2013, **5**, 6189–6200.
40 X. Zhang, C. Li and Y. Luo, *Langmuir*, 2011, **27**, 1915–1923.
41 Y. Si and E. T. Samulski, *Nano Lett.*, 2008, **8**, 1679–1682.
42 Y. Hana, M. Shen, Y. Wua, J. Zhu, B. Ding, H. Tong and X. Zhang, *Synth. Met.*, 2013, **172**, 21–27.